Density-Dependent Quantum Hall States and Zeeman Splitting in Monolayer and Bilayer WSe_2

Hema C. P. Movva,[1] Babak Fallahazad,[1] Kyounghwan Kim,[1] Stefano Larentis,[1] Takashi Taniguchi,[2] Kenji Watanabe,[2] Sanjay K. Banerjee,[1] and Emanuel Tutuc[1,*]
[1]Microelectronics Research Center, Department of Electrical and Computer Engineering, The University of Texas at Austin, Austin, Texas 78758, USA
[2]National Institute of Materials Science, 1-1 Namiki Tsukuba, Ibaraki 305-0044, Japan
(Received 10 February 2017; published 15 June 2017)

We report a study of the quantum Hall states (QHS) of holes in mono- and bilayer WSe_2. The QHS sequence transitions between predominantly even and predominantly odd filling factors as the hole density is tuned in the range $1.6–12 \times 10^{12}\ \mathrm{cm}^{-2}$. Measurements in tilted magnetic fields reveal an insensitivity of the QHS to the in-plane magnetic field, evincing that the hole spin is locked perpendicular to the WSe_2 plane. Furthermore, the QHS sequence is insensitive to an applied electric field. These observations imply that the QHS sequence is controlled by the Zeeman-to-cyclotron energy ratio, which remains constant as a function of perpendicular magnetic field at a fixed carrier density, but changes as a function of density due to strong electron-electron interaction.

DOI: 10.1103/PhysRevLett.118.247701

The strong spin-orbit coupling and broken inversion symmetry in $2H$ transition metal dichalcogenide (TMD) monolayers leads to coupled spin and valley degrees of freedom [1]. Breaking the time reversal symmetry by applying a perpendicular magnetic field further lifts the valley degeneracy, thanks to the spin (valley) Zeeman effect [2,3]. Insights into the Zeeman effect, a fundamental property of TMDs, have been provided by magneto-optical measurements of TMD monolayers, which report the exciton g factors from luminescence shifts in perpendicular magnetic fields [4,5]. Magnetotransport has been used to determine the effective carrier g factor (g^*) in several two-dimensional electron systems (2DESs) [6–8], and recent advances in sample fabrication have now facilitated detailed studies of the electron physics in TMDs [9–11]. Tungsten diselenide (WSe_2) is of particular interest because of a large spin-orbit splitting in the valence band [12], high-mobility [10], and low temperature Ohmic contacts [13]. Here we report a magnetotransport study of 2D holes in mono- and bilayer WSe_2, in the quantum Hall regime. The quantum Hall states (QHS) reveal interesting transitions between predominantly even and predominantly odd filling factors (FFs) as the hole density is tuned. Measurements in tilted magnetic fields reveal the QHS sequence is insensitive to the in-plane magnetic field, indicating that the hole spin is locked perpendicular to the WSe_2 plane. These observations can be explained by a Zeeman-to-cyclotron energy ratio which remains constant as a function of perpendicular magnetic field at a fixed carrier density, but changes as a function of density because of strong electron-electron interaction.

Figure 1(a) shows the schematic cross section, and Fig. 1(b) the optical micrograph of an h-BN encapsulated WSe_2 sample with bottom Pt contacts, and separate local top and back gates. The mono- and bilayer WSe_2 Hall bar samples were fabricated using a modified van der Waals assembly technique [13,14]. The bottom Pt electrodes in combination with a large, negative top-gate bias (V_{TG}) ensure Ohmic hole contacts to the WSe_2 [10,13]. Both V_{TG}, and a back-gate bias (V_{BG}) were used to tune the WSe_2 hole carrier density, p. The magnetotransport was probed using low frequency lock-in techniques at a temperature, $T = 1.5$ K, and magnetic fields up to $B = 35$ T. The p values at which we observe well-defined Shubnikov–de Haas (SdH) oscillations are in the range $1.6–12 \times 10^{12}\ \mathrm{cm}^{-2}$, as determined from the slope of the Hall resistance, and from the SdH oscillations minima. The weak interlayer coupling in bilayer WSe_2 allows a selection of the top or bottom layer to be populated with holes depending on the applied gate biases [10]. At negative V_{TG}, and positive V_{BG} only the top layer is populated, and the bilayer effectively acts as a monolayer, albeit with a dissimilar dielectric environment [15]. All the bilayer data presented here were collected under such biasing conditions, and are therefore closely similar to the monolayer data. In the range of densities probed, holes in both mono- and bilayer WSe_2 reside at the K (K') valley, thanks to the $K - \Gamma$ valley energy splitting of 640 meV and 80 meV in mono- and bilayer WSe_2, respectively [16]. The analysis of SdH data in our samples shows only one populated subband, with the same effective mass for both mono- and bilayer WSe_2 [10].

Figure 1(c) shows the longitudinal (R_{xx}) and Hall (R_{xy}) resistance vs perpendicular magnetic field (B) for a bilayer WSe_2 sample at the lowest density, $p = 1.6 \times 10^{12}\ \mathrm{cm}^{-2}$. The R_{xx} data show SdH oscillations starting at $B \cong 5$ T, which translates into a mobility $\mu \simeq 2000\ \mathrm{cm}^2/\mathrm{V\,s}$. The FFs, $\nu = ph/eB$, at the R_{xx} minima are marked; h is the

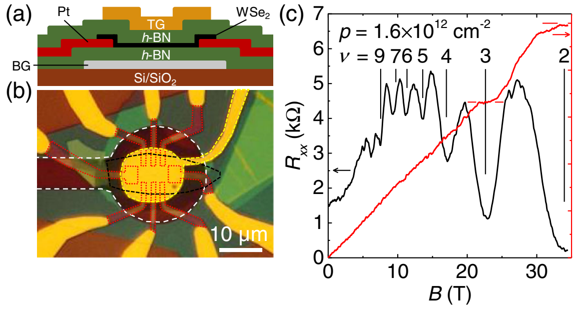

FIG. 1. (a) Schematic cross section of an h-BN encapsulated WSe_2 sample with bottom Pt contacts, a top gate (TG), and a local back gate (BG). (b) Optical micrograph of a typical WSe_2 Hall bar sample. The TG, Pt contacts, WSe_2 flake, and BG are outlined in yellow, red, black, and white dashed lines, respectively. (c) R_{xx} and R_{xy} vs B in bilayer WSe_2 measured at $T = 1.5$ K, and at the lowest hole density, $p = 1.6 \times 10^{12}$ cm^{-2}. The ν values at the R_{xx} minima are labeled. Quantized R_{xy} plateaus are observed at $\nu = 2, 3$.

Planck constant, and e the electron charge. The R_{xy} data show developed QHS plateaus at $\nu = 2, 3$, where R_{xy} is quantized at values of $h/\nu e^2$. The QHS occur at consecutive integer FFs ($\nu = 2, 3, 4, \ldots$) for $B > 10$ T, indicating a full lifting of the twofold Landau level (LL) degeneracy in WSe_2 [10]. For $B < 10$ T, the QHS occur at consecutive odd integer FFs ($\nu = 7, 9, \ldots$). In the following, we will use the term "QHS sequence," be it even or odd, to refer to the QHS FFs in the lower range of B values, such that the LL degeneracy is not fully lifted.

To better understand the QHS sequence, we performed magnetotransport measurements as a function of p in both mono- and bilayer WSe_2. Figures 2(a) and 2(b) show R_{xx} and R_{xy} vs B measured for the same bilayer sample discussed in Fig. 1 at $p = 3.9 \times 10^{12}$ cm^{-2}, and $p = 5.3 \times 10^{12}$ cm^{-2}, respectively. While the data at $p = 3.9 \times 10^{12}$ cm^{-2} show an odd QHS sequence, the QHS sequence is even at $p = 5.3 \times 10^{12}$ cm^{-2}. Figure 2(c) shows R_{xx} vs ν at various values of p from 6.1×10^{12} cm^{-2} to 2.4×10^{12} cm^{-2}. The data at $p = 6.1 \times 10^{12}$ cm^{-2} show strong R_{xx} minima at even FFs, and weakly developing minima at odd FFs for $\nu < 16$, hence, a predominantly even QHS sequence. As p is reduced to 4.4×10^{12} cm^{-2}, the minima at odd FFs become stronger, and equal in strength to the minima at even FFs. The QHS sequence at this p cannot be unambiguously classified as even or odd. Further reduction of p to 3.9×10^{12} cm^{-2} makes the odd FFs stronger than the even FFs, rendering the QHS sequence as predominantly odd. The odd QHS sequence is retained down to $p = 2.9 \times 10^{12}$ cm^{-2}. On further reduction of p to 2.4×10^{12} cm^{-2}, the QHS sequence reverts to even. Figure 2(d) shows a similar data set for monolayer WSe_2, where the QHS sequence transitions from even at $p = 9.7 \times 10^{12}$ cm^{-2} to odd at $p = 4.6 \times 10^{12}$ cm^{-2}, and back to even at $p = 3.3 \times 10^{12}$ cm^{-2}.

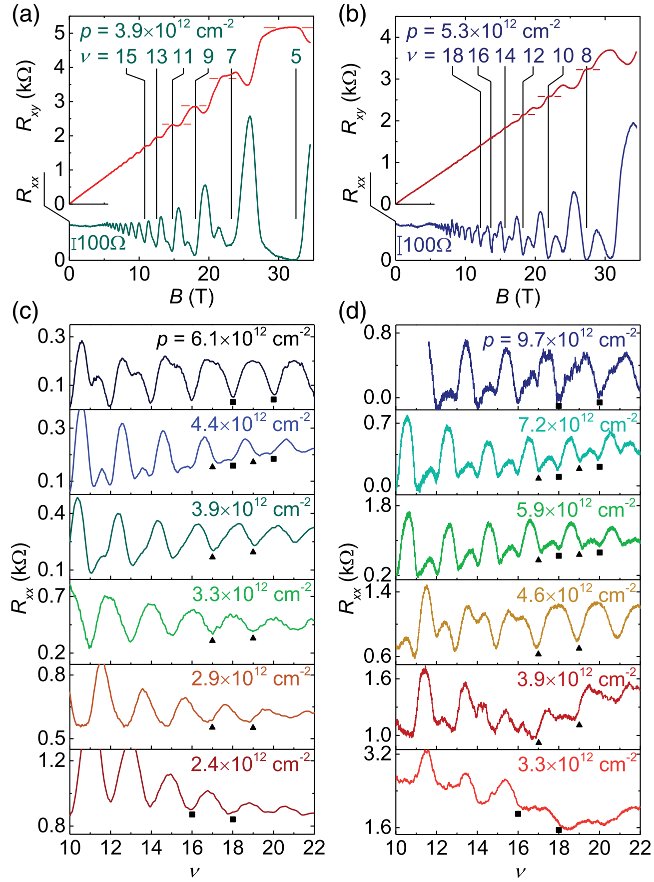

FIG. 2. (a),(b) R_{xx} and R_{xy} vs B in bilayer WSe_2 at $p = 3.9 \times 10^{12}$ cm^{-2} [panel (a)], showing QHS at predominantly odd FFs, and at $p = 5.3 \times 10^{12}$ cm^{-2} [panel (b)], showing QHS at predominantly even FFs. (c) R_{xx} vs ν in bilayer WSe_2 at different p values. The QHS sequence changes from even at $p = 6.1 \times 10^{12}$ cm^{-2} to odd at $p = 3.3 \times 10^{12}$ cm^{-2}, and back to even at $p = 2.4 \times 10^{12}$ cm^{-2}. (d) R_{xx} vs ν in monolayer WSe_2 at different p values show similar QHS sequence transitions. Representative R_{xx} minima at even and odd QHS are marked by square and triangle symbols, respectively, in panels (c),(d).

This unusual density-dependent QHS sequence suggests an interesting interplay of the LL Zeeman splitting and the cyclotron energy. The cyclotron energy of the LLs originating in the upper valence band of monolayer WSe_2 is $E_n = -n\hbar\omega_c$; n is the orbital LL index, $\hbar$ is the reduced Planck constant, $\omega_c = eB/m^*$ is the cyclotron frequency, $m^* = 0.45m_0$ the hole effective mass [10]; m_0 is the bare electron mass. The LLs with $n > 0$ are two-fold, spin-valley degenerate, whereas the $n = 0$ LL is non-degenerate [3,17]. Consequently, in the absence of LL Zeeman splitting, an odd QHS sequence is expected. However, if the LL spin degeneracy is lifted through a Zeeman splitting $E_Z = g^*\mu_B B$ comparable to the cyclotron energy $E_c = \hbar\omega_c$, the QHS sequence changes accordingly [18]; μ_B is the Bohr magneton. An E_Z/E_c ratio close to an even (odd) integer leads to a QHS sequence that is predominantly odd (even). Two noteworthy observations can be made based on Fig. 2 data. First, the presence of an even or odd QHS sequence at a fixed density implies that the E_Z/E_c ratio, and g^* do not change with B at low fields. Second, the different QHS transitions observed in Fig. 2 suggest that the E_Z/E_c ratio, and therefore g^* change with density, likely because electron-electron interaction associated with the large m^* in this system leads to an enhanced g^* as the density is reduced. We note that E_Z, and g^* include contributions from the electron spin and orbital magnetic moment, as well as interaction effects.

Two measurement types have been traditionally used to probe the Zeeman splitting in 2DESs. In a tilted magnetic field, the B component perpendicular to the 2DES plane ($B_\perp$) determines the cyclotron energy $E_c = \hbar\omega_c = \hbar e B_\perp/m^*$, while the Zeeman energy, $E_Z = g^* \mu_B B$ depends on the total field [19]. At specific angles θ between the B field and the normal to the 2DES plane, the E_Z/E_c ratio attains integer values, which leads to a collapse of different QHS, and allows a quantitative determination of E_Z. To assess this effect in our samples, Fig. 3(a) shows R_{xx} vs $B_\perp$ for a monolayer WSe_2 sample, measured at $p = 4.6 \times 10^{12}$ cm^{-2}, and at different values of θ. The R_{xx} at $\theta = 0°$ shows an odd QHS sequence, which remains virtually unchanged for all values of θ up to 77°. A similar behavior was observed even for bilayer WSe_2, suggesting indeed that E_Z is *insensitive* to the parallel component of the B field ($B_{||}$) in both mono- and bilayer WSe_2. This observation is in stark contrast to the vast majority of 2DESs explored in host semiconductors such as Si [6,19], GaAs [7], AlAs [8], black phosphorus [20], and bulk WSe_2 [11].

A second technique used to determine E_Z is the magnetoresistance measured as a function of the magnetic field parallel to the 2DES plane. The Zeeman coupling leads to a spin polarization of the 2DES, which reaches unity when E_Z is equal to the Fermi energy. Experimentally, R_{xx} vs $B_{||}$ measured at $\theta = 90°$ shows a positive magnetoresistance, along with a saturation or a marked kink at the B field corresponding to full spin polarization [7,8,21,22]. Figure 3(b) shows R_{xx} vs $B_{||}$ data for the monolayer sample of Fig. 3(a). Surprisingly, yet consistent with Fig. 3(a) data, R_{xx} remains constant over the entire range of $B_{||}$, which implies that E_Z depends only on $B_\perp$, namely, $E_Z = g^* \mu_B B_\perp$, via a density-dependent g^*. The insensitivity of E_Z to $B_{||}$ indicates that the hole spin at the K (K') valley is locked perpendicular to the plane, a direct consequence of the strong spin-orbit coupling, and mirror symmetry in monolayer WSe_2 [12]. Optical experiments on monolayer WSe_2 have shown a similar insensitivity of E_Z to $B_{||}$ [5]. We note that spin-locking along the z direction renders the tilted B-field technique ineffective to determine E_Z.

In light of Fig. 2 data which suggest a density-dependent g^*, one important question is whether the g^* variation is determined by the density, or by the applied transverse electric field (E), which depends on the applied gate biases

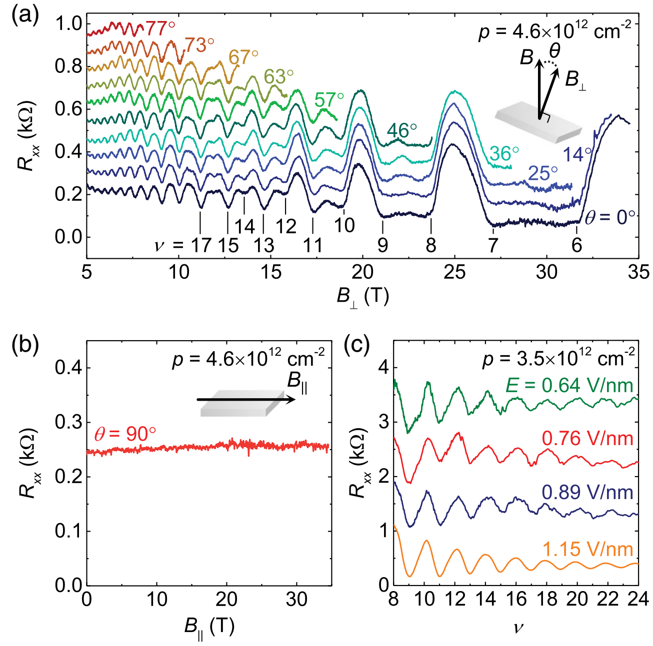

FIG. 3. (a) R_{xx} vs $B_\perp$ in monolayer WSe_2 at $p = 4.6 \times 10^{12}$ cm^{-2}, and at different θ values. The traces are offset for clarity. Inset: Schematic of the sample orientation with respect to the B field. (b) R_{xx} vs $B_{||}$ corresponding to the $\theta = 90°$ trace of panel (a) data. The R_{xx} remains unchanged in the entire B-field range. (c) R_{xx} vs ν measured in bilayer WSe_2 at $p = 3.5 \times 10^{12}$ cm^{-2}, and at different E-field values. The traces are offset for clarity.

and can change concomitantly with the density. The impact of a transverse E field on band structure has been experimentally investigated, among others, in 2D electrons in InGaAs/InAlAs [23], 2D holes in GaAs [24], and has been theoretically considered in TMDs using a Bychkov-Rashba coupling [25]. To probe the impact of the E field on the QHS sequence in WSe_2, we performed R_{xx} vs B measurements by varying $E = |C_{TG}V_{TG} - C_{BG}V_{BG}|/2\epsilon_0$ at constant p; C_{TG} (C_{BG}) is the top (back)-gate capacitance, and ϵ_0 the vacuum permittivity. Figure 3(c) shows R_{xx} vs ν measured in bilayer WSe_2 at $p = 3.5 \times 10^{12}$ cm^{-2}, at different values of E. The data show no variation of the QHS sequence when the E field varies from 0.64 V/nm to 1.15 V/nm. By comparison, the E field changes from 0.92 V/nm to 1.11 V/nm in Fig. 2(c), concomitantly with the density change from 6.1×10^{12} cm^{-2} to 3.9×10^{12} cm^{-2}, a range in which a QHS sequence transition from even to odd is observed. Based on these observations, we rule out the effect of the E field on g^*, and in turn, on the QHS sequence.

In Fig. 4(a), we summarize the QHS sequence vs p for four monolayer, and four bilayer WSe_2 samples. The data points are grouped into an even or odd QHS sequence over a range of p. We attribute the QHS sequence transitions to a change in the E_Z/E_c ratio with varying p. For instance, $E_Z \approx E_c$ ($E_Z \approx 2E_c$) can lead to an even (odd) QHS

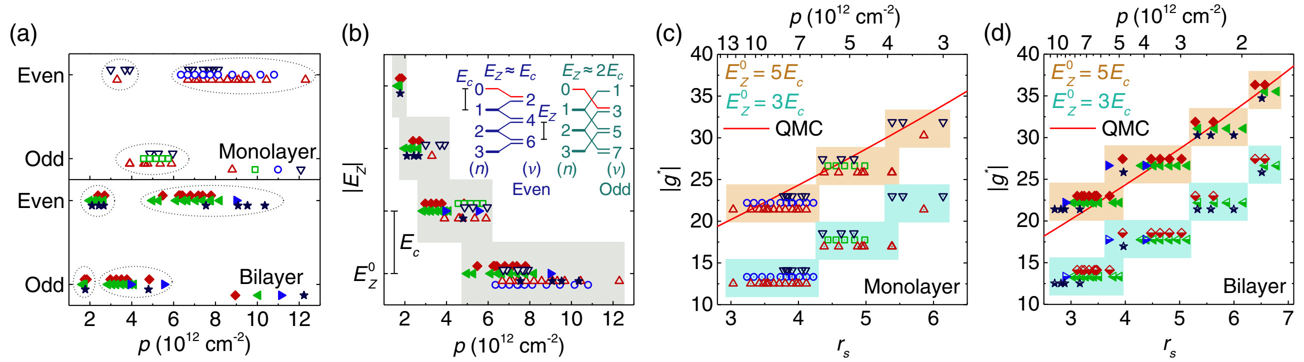

FIG. 4. (a) QHS sequence vs p for four monolayer (top, open symbols), and four bilayer (bottom, solid symbols) WSe_2 samples. The dotted lines group the data points belonging to the same QHS sequence in a given p range. (b) Panel (a) data converted to $|E_Z|$ vs p, assuming an $|E_Z|$ increment of E_c for every QHS sequence transition in the direction of decreasing p. The inset shows two possible scenarios where the QHS sequence could be even ($E_Z \approx E_c$) or odd ($E_Z \approx 2E_c$). (c) Monolayer, and (d) bilayer WSe_2 $|g^*|$ vs r_s (bottom axis) or p (top axis) for $E_Z^0 = 5E_c$ (open, solid symbols), $E_Z^0 = 3E_c$ (dotted, half-filled symbols), and the QMC calculation for $g_b = 8.5$ (line). The symbols within a group are vertically offset for clarity. The shaded regions correspond to a $\pm E_c/2$ error bar in panel (b) and a $\pm\Delta g^*/2$ error bar in panels (c),(d).

sequence [Fig. 4(b) inset]. Generalized further, $|E_Z|/E_c \in [2k-1/2, 2k+1/2]$ yields an odd QHS sequence, and $|E_Z|/E_c \in [2k+1/2, 2k+3/2]$ yields an even QHS sequence; k is an integer. Each of the groups of Fig. 4(a) can therefore be assigned an $|E_Z|$ within a $[-E_c/2, E_c/2]$ window. Starting with $|E_Z| = E_Z^0$ at the highest value of p probed, and assuming $|E_Z|$ increases with reducing p because of interaction, we can assign an $|E_Z|$ increment of E_c for every QHS sequence transition in the direction of decreasing p [Fig. 4(b)]. In the absence of electron-electron interaction, the g factor, referred to as the band g factor (g_b), is determined by the material band structure. Exchange interaction can enhance g_b to a value g^*, which increases with decreasing density, an observation reported for several 2DESs in Si [6,21], GaAs [7], and AlAs [8]. The interaction strength is gauged by the dimensionless parameter, $r_s = 1/(\sqrt{\pi p}a_B^*)$, the ratio of the Coulomb energy to the kinetic energy; $a_B^* = a_B(\kappa m_0/m^*)$, a_B is the Bohr radius, and κ is the effective dielectric constant of the medium surrounding the 2DES.

The $|E_Z|$ vs p of Fig. 4(b) can therefore be converted to a $|g^*|$ vs r_s dependence. We first address the value of $E_Z^0 = g_0^*\mu_B B$. The even QHS sequence at the highest p probed implies that $E_Z^0 = (2k+1)E_c$, or equivalently, $g_0^* = 4.44(2k+1)$; k is an integer [26]. Recent magneto-reflectance measurements that resolve the LL spectrum report a $g_b = 8.5$ for holes in monolayer WSe_2 [27]. To account for the uncertainty in E_Z^0, we consider two scenarios of g_0^* corresponding to $k = 1$ ($E_Z^0 = 3E_c$), and $k = 2$ ($E_Z^0 = 5E_c$). We rule out the case $k = 0$ based on the reported g_b value [27]. The E_c-step increments of $|E_Z|$ between groups are equivalent to a $|g^*|$ increment of $\Delta g^* = 2m_0/m^* = 4.44$ [26]. Within this framework, Fig. 4(c) and Fig. 4(d) show $|g^*|$ vs r_s for the mono- and bilayer samples, respectively. Because of the difference in dielectric environment, slightly different κ values were used to convert p into r_s for mono- and bilayer WSe_2 [28]. For comparison, in Figs. 4(c) and 4(d) we include the g_b value multiplied by the interaction enhanced spin susceptibility obtained from quantum Monte Carlo (QMC) calculations [32]. The QMC calculations along with the g_b of Ref. [27] match well with $|g^*|$ determined using $E_Z^0 = 5E_c$ for both mono- and bilayer WSe_2. It is noteworthy that the relatively large $m^* = 0.45m_0$ leads to moderately large r_s values, and potentially strong interaction effects even at high carrier densities [33].

In summary, we present a density-dependent QHS sequence of holes in mono- and bilayer WSe_2, which transitions between even and odd filling factors as the hole density is tuned. The QHS sequence is insensitive to the in-plane B field, indicating that the hole spin is locked perpendicular to the WSe_2 plane, and is also insensitive to the transverse E field. The QHS sequence transitions stem from an interplay between the cyclotron and Zeeman splittings via an enhanced g^* due to strong electron-electron interaction.

We thank X. Li, K. F. Mak, and F. Zhang for technical discussions. We also express gratitude to D. Graf, J. Jaroszynski, and A. V. Suslov for technical assistance. We acknowledge support from NRI SWAN, National Science Foundation Grant No. EECS-1610008, and Intel Corp. A portion of this work was performed at the National High Magnetic Field Laboratory, which is supported by National Science Foundation Cooperative Agreement No. DMR-1157490, and the State of Florida.

H. C. P. M. and B. F. contributed equally to this work.

*etutuc@mer.utexas.edu

[1] D. Xiao, G.-B. Liu, W. Feng, X. Xu, and W. Yao, Phys. Rev. Lett. **108**, 196802 (2012).

[2] T. Cai, S. A. Yang, X. Li, F. Zhang, J. Shi, W. Yao, and Q. Niu, Phys. Rev. B **88**, 115140 (2013).

[3] F. Rose, M. O. Goerbig, and F. Piéchon, Phys. Rev. B **88**, 125438 (2013).

[4] Y. Li *et al.*, Phys. Rev. Lett. **113**, 266804 (2014); G. Aivazian, Z. Gong, A. M. Jones, R.-L. Chu, J. Yan, D. G. Mandrus, C. Zhang, D. Cobden, W. Yao, and X. Xu, Nat. Phys. **11**, 148 (2015); D. MacNeill, C. Heikes, K. F. Mak, Z. Anderson, A. Kormányos, V. Zólyomi, J. Park, and D. C. Ralph, Phys. Rev. Lett. **114**, 037401 (2015); A. A. Mitioglu, P. Plochocka, Á. Granados del Aguila, P. C. M. Christianen, G. Deligeorgis, S. Anghel, L. Kulyuk, and D. K. Maude, Nano Lett. **15**, 4387 (2015); G. Wang, L. Bouet, M. M. Glazov, T. Amand, E. L. Ivchenko, E. Palleau, X. Marie, and B. Urbaszek, 2D Mater. **2**, 034002 (2015); A. V. Stier, N. P. Wilson, G. Clark, X. Xu, and S. A. Crooker, Nano Lett. **16**, 7054 (2016).

[5] A. Srivastava, M. Sidler, A. V. Allain, D. S. Lembke, A. Kis, and A. Imamoğlu, Nat. Phys. **11**, 141 (2015).

[6] A. A. Shashkin, S. V. Kravchenko, V. T. Dolgopolov, and T. M. Klapwijk, Phys. Rev. Lett. **87**, 086801 (2001).

[7] J. Zhu, H. L. Stormer, L. N. Pfeiffer, K. W. Baldwin, and K. W. West, Phys. Rev. Lett. **90**, 056805 (2003).

[8] K. Vakili, Y. P. Shkolnikov, E. Tutuc, E. P. De Poortere, and M. Shayegan, Phys. Rev. Lett. **92**, 226401 (2004).

[9] X. Cui *et al.*, Nat. Nanotechnol. **10**, 534 (2015); Z. Wu *et al.*, Nat. Commun. **7**, 12955 (2016).

[10] B. Fallahazad, H. C. P. Movva, K. Kim, S. Larentis, T. Taniguchi, K. Watanabe, S. K. Banerjee, and E. Tutuc, Phys. Rev. Lett. **116**, 086601 (2016).

[11] S. Xu *et al.*, Phys. Rev. Lett. **118**, 067702 (2017).

[12] Z. Zhu, Y. Cheng, and U. Schwingenschlögl, Phys. Rev. B **84**, 153402 (2011).

[13] H. C. P. Movva, A. Rai, S. Kang, K. Kim, B. Fallahazad, T. Taniguchi, K. Watanabe, E. Tutuc, and S. K. Banerjee, ACS Nano **9**, 10402 (2015).

[14] K. Kim *et al.*, Nano Lett. **16**, 1989 (2016).

[15] While a monolayer has only h-BN as the bottom dielectric, a bilayer biased to populate only the top layer has an unpopulated WSe_2 bottom layer, which alters the dielectric environment of holes in the top layer.

[16] M. Yankowitz, D. McKenzie, and B. J. LeRoy, Phys. Rev. Lett. **115**, 136803 (2015); C. Zhang, Y. Chen, A. Johnson, M.-Y. Li, L.-J. Li, P. C. Mende, R. M. Feenstra, and C.-K. Shih, Nano Lett. **15**, 6494 (2015); Y. Zhang *et al.*, Nano Lett. **16**, 2485 (2016).

[17] X. Li, F. Zhang, and Q. Niu, Phys. Rev. Lett. **110**, 066803 (2013).

[18] R.-L. Chu, X. Li, S. Wu, Q. Niu, W. Yao, X. Xu, and C. Zhang, Phys. Rev. B **90**, 045427 (2014).

[19] F. F. Fang and P. J. Stiles, Phys. Rev. **174**, 823 (1968).

[20] L. Li *et al.*, Nat. Nanotechnol. **11**, 593 (2016).

[21] T. Okamoto, K. Hosoya, S. Kawaji, and A. Yagi, Phys. Rev. Lett. **82**, 3875 (1999).

[22] E. Tutuc, E. P. De Poortere, S. J. Papadakis, and M. Shayegan, Phys. Rev. Lett. **86**, 2858 (2001).

[23] J. Nitta, T. Akazaki, H. Takayanagi, and T. Enoki, Phys. Rev. Lett. **78**, 1335 (1997).

[24] J. P. Lu, J.-B. Yau, S. P. Shukla, M. Shayegan, L. Wissinger, U. Rössler, and R. Winkler, Phys. Rev. Lett. **81**, 1282 (1998); R. Winkler, E. Tutuc, S. J. Papadakis, S. Melinte, M. Shayegan, D. Wasserman, and S. A. Lyon, Phys. Rev. B **72**, 195321 (2005).

[25] A. Kormányos, V. Zólyomi, N. D. Drummond, and G. Burkard, Phys. Rev. X **4**, 011034 (2014).

[26] We assume a density independent $m^* = 0.45m_0$ [10].

[27] Z. Wang, J. Shan, and K. F. Mak, Nat. Nanotechnol. **12**, 144 (2017).

[28] For a 2DES with an asymmetric dielectric environment, $\kappa(t,b) = [(\epsilon_t^{||}\epsilon_t^{\perp})^{1/2} + (\epsilon_b^{||}\epsilon_b^{\perp})^{1/2}]/2$; $\epsilon_{t(b)}^{||/\perp}$ are the top (bottom) medium dielectric constants. For monolayer WSe_2, $\kappa = \kappa(h\text{-BN}, h\text{-BN})$. For bilayer WSe_2 [15], $\kappa = [\kappa(h\text{-BN}, h\text{-BN}) + \kappa(h\text{-BN}, WSe_2)]/2$. We use $\epsilon_{h\text{-BN}}^{||} = 3.0$, $\epsilon_{h\text{-BN}}^{\perp} = 6.9$ [29], $\epsilon_{WSe_2}^{||} = 7.2$ [30], and $\epsilon_{WSe_2}^{\perp} = 14$ [31].

[29] R. Geick, C. H. Perry, and G. Rupprecht, Phys. Rev. **146**, 543 (1966).

[30] K. Kim, S. Larentis, B. Fallahazad, K. Lee, J. Xue, D. C. Dillen, C. M. Corbet, and E. Tutuc, ACS Nano **9**, 4527 (2015).

[31] Y. Li, A. Chernikov, X. Zhang, A. Rigosi, H. M. Hill, A. M. van der Zande, D. A. Chenet, E.-M. Shih, J. Hone, and T. F. Heinz, Phys. Rev. B **90**, 205422 (2014).

[32] C. Attaccalite, S. Moroni, P. Gori-Giorgi, and G. B. Bachelet, Phys. Rev. Lett. **88**, 256601 (2002).

[33] B. Tanatar and D. M. Ceperley, Phys. Rev. B **39**, 5005 (1989).